Characterization and Application of Nanomaterials (2023) Volume 6 Issue 1
doi:10.24294/can.v6i1.1852

ORIGINAL RESEARCH ARTICLE

Construction of semiclassical interatomic B–B pair potential to characterize all-boron nanomaterials

Levan Chkhartishvili

Engineering Physics Department, Georgian Technical University, Tbilisi 0160, Georgia. E-mail: levanchkhartishvili@gtu.ge

ABSTRACT

The semiclassical boron–boron interatomic pair potential is constructed in an integral form allowing its converting into the analytical one. It is an ab initio B–B potential free of any semiempirical adjusting parameters, which would serve as an effective tool for the theoretical characterization of all-boron and boron-rich nanomaterials.

Keywords: Interatomic Potential; Semiclassical Approach; Ground State Parameters; Nanomaterial; Boron

ARTICLE INFO

Received: 10 December 2022
Accepted: 6 February 2023
Available online: 17 February 2023

1. Introduction

Currently, the prospective wide technological applications of borophenes and boron-rich nanomaterials in general are of special research interests due to their variable interatomic bonding mechanism and related unique complex of physical and chemical properties (see some of recent reviews[1–6]). Among them, the small all-boron clusters B_n (containing $n < 20$ atoms) preferring (quasi) planar structures play an important role in characterization of borophenes and other 2D boron nanomaterials as can serve for their building blocks[7].

Boron nanoclusters' ground state parameters—bond lengths, specific (per atom) binding energy, atomic vibration frequencies, etc.—can be estimated on the basis of interatomic B–B pair potentials depended on a few rigorously chosen semiempirical parameters—see the paper and also the review of Chkhartishvili[8,9] which summarize results of similar attempts. Same approach has been found useful for the characterization of the relative stability of small (quasi) planar boron clusters, including the most abundant species B_{11}, B_{12}, and B_{13} in different charge states[10,11].

As is known, to study molecular properties quantitatively, e.g., determining the spectroscopic data or performing the collision calculations, potential curves of diatomic molecules are useful in analytical form. Analytical pair interatomic potential curves are also needed to deduce the polyatomic molecular curves. In view of this, in the present work, we demonstrate how it is possible based on semiclassical approach to construct the B–B interatomic pair potential in an integral form, which is reducible to the analytical one. Paper is organized as follows. After this introduction, there is given a short review on interatomic potentials in general. Then charge density and potential distributions in boron atom are described semiclassically. They are used to construct the B–B interaction potential energy curve in an integral form. And finally, based on discussion of obtained results some conclusions are drawn.

2. Interatomic potentials

When developing the numerical physical model of a material, the ab initio approaches, such as the DFT (Density Functional Theory) or QC (Quantum Chemistry), providing the best accuracy on its electronic properties is limited to fragments up to thousands of atoms. To larger systems, it should be employed the computations by classical MD (Molecular Dynamics), MC (Monte Carlo) or FE (Finite Element) methods, which are much faster but less accurate and assume that constituent atoms are solid spheres influenced by interactions and in a good approximation follow the classical equations of motion.

Then behavior of materials in the elastic, electric or magnetic force fields depends on type and energy of interatomic bonding and the general understanding of their properties can be based on interaction potentials between atoms or ions[12]. The (long-range) interatomic forces, i.e., gradients of interatomic potentials prescribed as functions of atomic coordinates, play key role in capillarity and wetting phenomena as well[13]. The choice of forms or these potentials depends on the particular problem features. Recent Special Issue of the journal *Molecules*: "Intermolecular forces: From atoms and molecules to nanostructures"[14] has been devoted the relationship between forces acting between the atomic system particles and its properties across different scales: from molecules, simple aggregates or small clusters to nanostructures and other types of condensed matter at the mesoscale. The parameters of introduced types of interatomic potentials can be derived both from experiments or quantum mechanics.

To understand molecules chemical properties and also for their force fields high-quality empirical parameterization, the obtaining of accurate conformational energetics is of significance. Molecule conformational energy includes strain energy coming from bond distortions, valence angles, torsion strains, etc., and enables to describe deviations of actual molecular geometry from the ideal one. As for intermolecular forces, they control most of the properties of the materials, such as their existence in solid, liquid or gaseous states, relative stability and chemical reactivity.

The ab initio potentials are found in DFT or electron gas approximations, in which various contributions in the multi-atomic system energy—Coulomb, kinetic, exchange, correlation, etc.—are additively taken into account. In this case, in calculating the interaction potentials for heteroatomic systems, it is more correct to use a separate combination of these types of contributions.

Recent alternative to both empirical and ab initio interatomic potentials are ML (Machine Learning) potentials. ML is becoming a method of choice for modeling complex chemical processes and materials providing a surrogate model trained on a reference dataset that can be used to establish a relationship between molecular structure and chemical properties. ML trained on quantum mechanical calculations is a powerful tool for modeling the PES (Potential Energy Surface). A critical factor for the automated discovery of robust interatomic potentials by ML is the quality and diversity of the training dataset.

The course to atomistic simulations[15] provides classification of popular interatomic potentials; their characterization in terms of accuracy, transferability and computational speed; potential cut-off procedures; short review of potentials used in MD and MC methods; derivation of the force from pair potential and force fields in materials; relationship between pair potential and elastic constants; limitations of pair potentials; and description of pair potentials versus many-atomic potentials.

The NIST's (National Institute of Standards and Technology) IPR (Interatomic Potentials Repository)[16] serves for a source of interatomic potentials and force fields, in which there are presented all the possible classes of potentials and materials (metals, semiconductors, oxides and carbon-containing systems). Interatomic and also fictional potentials are provided both for elementary and non-elementary (alloys and compounds) materials. It is specially noted that: (i) multicomponent potentials may not be applicable to the full composition range; (ii) coarse-grained poten-

tials reduce the simulation complexity by representing molecular or alloy compositions with a single particle type; and (iii) fictional potentials purposefully fitted to target properties are not able to represent real materials accurately.

2.1 Empirical potentials

Interactions between atoms can be modeled using different two- or many-atomic potentials. The total interaction potential can be written as a series of terms depending on the position of one, two, three, … atoms at a definite moment of time: $U_{\text{total}}(\vec{r}_1, \vec{r}_2, \vec{r}_3, \ldots) = \sum_i U_1(\vec{r}_i) + \sum_{ij} U_2(\vec{r}_i, \vec{r}_j) + \sum_{ijk} U_3(\vec{r}_i, \vec{r}_j, \vec{r}_k) + \cdots$. Here $\vec{r}_1, \vec{r}_2, \vec{r}_3, \ldots$ are the radius-vectors of atoms and $U_1, U_2, U_3, \ldots$—one-, two-, three-atomic, … potentials, respectively. The term U_1 is an atom's potential in self-consistent or external force field.

As for the term U_2, in the simplest ionic bonding model, it is expressed by the potential energy of Coulomb or electrostatic interaction between a pair of oppositely charged ions: $U_{\text{C}}(r) = -A/r$, where $A > 0$ is the constant dependent on effective point charges of interacting atomic ions and $r = |\vec{r}_1 - \vec{r}_2|$ is the distance separating them. The Madelung or electrostatic energy of an ionic crystal is the sum of potential energies of interaction between constituent ions. A negative overall energy implies attraction and then system's stability.

Electrostatic attraction between cations and anions increases as they approach each other, until at some distance their electron clouds begin to overlap leading to repulsion. These two forces of opposite signs are balanced at equilibrium separation. The repulsive energy typically is formulated as $U_{\text{R}}(r) = B/r^n$, where $B > 0$ and $n > 0$ are the empirical constants. Bond length and binding energy can be determined by minimizing the total potential energy: $U(r) = U_{\text{C}}(r) + U_{\text{R}}(r) = B/r^n - A/r$. Alternatively, the repulsion can be expressed by the Born–Mayer potential: $U_{\text{B-M}}(r) = C\exp(-r/a)$ with $C > 0$ and $a > 0$ for constants.

Usually, the interatomic potentials obtained empirically are approximated by model potentials without separation of terms with clear physical sense. These are Lennard–Jones $U_{\text{LJ}}(r) = B/r^{12} - A/r^6$, Morse $U_{\text{M}}(r) = D(\exp(-2\alpha(r-a) - \exp(-\alpha(r-a))$, Buckingham $U_{\text{B}}(r) = C\exp(-r/a) - A/r^6$, … potentials including two more positive parameters: D and α.

Sometimes, the Lennard–Jones potential, which is frequently used for modeling rare gas crystals bounded by van der Waals forces, is presented as $U_{\text{LJ}}(r) = 4D((r_0/r)^{12} - (r_0/r)^6)$, where r_0, called as van der Waals diameter, is the value of r, when $U_{\text{LJ}}(r)$ function is zero, and D is the potential well depth. The origin of such interatomic interaction can be imagined as interplay between van der Waals attraction and Pauli repulsion related to zero point fluctuations of electrons leading to induced dipole forces and their short-range interaction due to exclusion principle, respectively.

An important special form of $U_{\text{LJ}}(r)$ is the Mie–Lennard–Jones potential: $U_{\text{M-LJ}}(r) = (D/(b-a))\left(a(r_{\min}/r)^b - b(r_{\min}/r)^a\right)$, where D and $r_{\min}$ denote depth and coordinate of the potential minimum, a and b are the numerical parameters, $1 < a < b$, characterizing long-range action and rigidity of the potential.

To construct adequate theoretical model for a material, it is necessary to use the empirical potentials that correctly take into account all the available types of interactions in a wide range of interatomic distances. In the simplest case, the pair interatomic potential can be chosen in the form of $U(r) = D(X(r)^2 - 2X(r))$, where $X(r)$ is some function of distance r. The first term takes into account the repulsion, while the second—the attraction of atoms. The expediency of choosing this approximation is due to following reasons. It, firstly, quite adequately describes the pair interaction energy dependence on the interatomic distance and, secondly, allows one to obtain the widely used analytical formulas for interaction potential energies and forces between systems of atoms, in particular, above mentioned Lennard–Jones and Morse potentials. The use of the Lennard–Jones potential leads to simple and easy-to-calculate explicit relations that describe the physical properties, such as the potential energy of sol-

id structure, liquid surface tension and solid surface energies, and heat of sublimation. Its disadvantage is the power-law dependence of the repulsion energy, which gives too fast fall as the distance increases. Morse potential, which takes into account the repulsive forces "softness", is deprived of this shortcoming and preferable to be used in modeling interactions in nanosystems, as well as quantum mechanical calculations since it allows one to obtain Schrodinger equation solutions in an explicit form. In the vicinity of minimum, any pair interaction potential is represented as a parabolic dependence $U(r) = -D + k(r - r_{\min})^2/2$, where k is the bond stiffness factor. In various solid state physics applications, it turns out to be useful the Mie–Lennard–Jones potential, whose parameters for most of elements of the Periodic Table were estimated by Magomedov[17]. The potential well depth D and equilibrium distance $r_{\min}$ values were calculated from heat of sublimation and the lattice constant or molar volume.

To estimate the pair interaction potential of different atoms, it can be used the Lorentz–Berthelot empirical combination rules: $U_{\min} \to U_{AB} = \sqrt{U_A U_B}$ and $r_{\min} \to r_{AB} = (r_A + r_B)/2$, where indices A and B denote the interacting atoms.

Three-atomic term U_3 frequently is expressed by the Tersoff potential:

$$U_T(\vec{r}_1, \vec{r}_2, \vec{r}_3) = (1/2) \sum_{i \neq j} f_c(r_{ij}) \left(a_{ij} f_a(r_{ij}) + b_{ij} f_r(r_{ij}) \right)$$

where $r_{ij} = |\vec{r}_i - \vec{r}_j|$ is the distance separating i and j atoms, $f_a(r) = -\alpha \exp(-\lambda_\alpha r)$ is the attractive three-atomic potential and $f_r(r) = \rho \exp(-\lambda_\rho r)$ is the repulsive two-atomic term (here parameters α, λ_α, ρ and λ_ρ are the positive constants), while $f_c(r)$ is a smooth cutoff function. The three-atomic contributions arise due to the bond-order parameters a_{ij} dependent on bonds length and angle between them. The parameters b_{ij} limiting the repulsive interactions range can be chosen as functions only of bonds length.

The most recent comprehensive review of empirical interatomic potentials designed to reproduce materials elastic properties, defect energies, bond formation and breaking, redox reactions, etc., has been done in the study of Muser *et al.*[18]. There are described the most popular two-atomic potentials such as: embedded-atom model potential for metals, bond-order potential for covalently bonded semiconductors, polarizable potentials including ionic systems of atoms, and quantum-Drude oscillator model potential mimicking multi-atomic dispersion. Emphasis is laid on the constraints ensue from the functional form of a potential. The review highlights potentials with simple functional forms allowing the analytical treatment. Below, some of interesting examples of practical applications of the empirical potentials are given.

Periodic Table's carbon subgroup elements—C, Si, Ge, Sn and Pb—are of interests because of occurring of the covalent-to-metallic bond-type transition. The available experimental data were used[19] to obtain the parameters of their pair interatomic potentials represented in the Mie–Lennard–Jones form. All the different approaches suggested for the self-consistent determination have same disadvantage: it is unclear whether it is correct or not to use the parameters obtained for a free atoms pair for double covalent bond in a crystal. To answer this question, it was investigated the evolution of the potential depth D value experimentally determined from the crystal properties during the covalent-to-metallic bond-type transition and demonstrated that D of a covalent bond determined from the bulk modulus is approximately twice the value which follows from the crystal atomization energy. A conclusion was drawn about the covalent bonding nature: such bond between in a crystal is double and these two bonds differ in potential depth value. Each of the generalized valence electrons realizes strong and weak bonds with own and alien ions, respectively. A double covalent bond under elastic, i.e., reversible, deformation of the crystal is about twice stronger than in the case of its sublimation, i.e., its destruction, because two valence electrons cannot depart from each other without breaking the weaker one. Bonds of both types are active at elastic deformation, but only weak bonds break at

plastic one, i.e., irreversible deformation. This explains the covalent crystals high brittleness along with their high strength. Recently, based on paired covalent bond model, it has been determined[20] that the causes of both the appearance of surface cracks on a semiconductor crystal at temperature T below its brittle-to-plastic transition point T_{bpt}, $T < T_{\mathrm{bpt}}$, and such transition at $T > T_{\mathrm{bpt}}$. At small deformations of a covalent crystal, it is energetically preferable to create a surface by irreversible rupture, than by reversible stretching. The brittle–plastic transition in elemental covalent crystals would accompanied by the surface covalent bonds metallization. It is shown that the transition temperature under static loads has an upper limit: $T_{\mathrm{bpt}}/T_{\mathrm{m}} < 0.45$, where T_{m} is the melting temperature. Thus, an analytical (i.e., without computer simulation) method was suggested for calculating the brittle–plastic transition temperature for elemental covalent crystals.

To overcome some drawbacks of previous determinations of four parameters characterizing the Mie–Lennard–Jones potential as applied to crystals, a different parameterization method was introduced by Magomedov[21]. It is based on the best agreement of the crystal thermoelastic properties calculated values from experimental data such as: crystal sublimation energy at zero temperature, thermal expansion coefficient and isothermal elasticity modulus at room temperature, and pressure–volume dependence according to the equation of state's room temperature isotherm curve. Method verification for iron Fe and gold Au showed good results, as well as its application for accurate calculation of some refractory metals (such as niobium Nb, tantalum Ta, molybdenum Mo and tungsten W) Debye temperature and sublimation and surface energies. Disordered Au–Fe substitution alloys were studied by Magomedov[22]. Namely, based on Mie–Lennard–Jones-type interatomic potential parameters, Au and Fe fcc (face-centered cubic) and bcc (body-centered cubic) structures were analytically determined, and the composition dependences of the Au–Fe alloys properties at the fcc–bcc structural phase transition were found. Then, the key parameters of activation processes were calculated[23] in various structures of iron. These are: Gibbs energy, enthalpy, entropy, and volume both for processes of formation of electrically neutral vacancies and self-diffusion of atoms.

A beryllium–tungsten Be–W interatomic potential was derived[24] using a formalism originated from the Pauling bond order concept. It found to be suitable for simulation of plasma–wall interactions (Be surface with W atom and vice versa) taking place in fusion reactor. Obtained interaction energies are qualitatively similar to that from ab initio, namely, DFT calculations showing that diffusion of Be into bulk W is not energetically favorable and the opposite is true for the reversed system. This Be–W potential can reasonably describe $\mathrm{Be}_x\mathrm{W}_y$ molecules with $x, y = 1, 2, 3, 4$ and intermetallic phases $\mathrm{Be_2W}$ and $\mathrm{Be_{12}W}$ as well.

A correlation between binding energy of an individual atom in metal lattice and its macroscopic parameters like Debye temperature, Young's modulus and sound speed was considered in the study of Erokhin and Kalashnikov[25]. Based on the Lennard–Jones potential, the anharmonic zero-point oscillations of a crystal were analyzed[26] within the framework of the diatomic model. It is shown that their amplitude cannot exceed the limiting value which is a certain part of the equilibrium interatomic distance. The compression of a crystal decreases the zero oscillations amplitude, while the tension increases it. It was found that crystal melting point depends on the de Boer parameter. The processes of melting and solidification of gold nanoclusters consisting of 43–1,055 atoms were studied[27] using the MC method and the Gupta multiatomic potential. It was shown that the temperature-dependences of the specific internal energy potential part and average first coordination number have pronounced hysteresis.

The work previously carried out in the context of quantitative crystal engineering involving the analysis of intermolecular interactions such as carbon (tetrel), pnicogen, chalcogen, and halogen bonding using experimental charge density methodology has been reviewed by Thomas *et al.*[28]. The focus was to extract electron density distribution in the intermolecular space and to obtain

guidelines to evaluate the strength and directionality of such interactions towards the design of molecular crystals with desired properties. In this formalism, the atomic electron density is divided into three terms: spherical core and spherical and asperical valence electron densities. It was demonstrated power and limits of X-ray diffraction experimental analysis using the CDMM (Charge Density Multipole Modeling) approach.

Using the continuum approximation for interacting atoms and the Mie–Grüneisen Theory, a simple equation of state for a monatomic crystal was constructed[29], which describes the phase diagram even in the vicinity of the critical point. The use of the Lennard–Jones formula for a pair potential made it possible to analytically find expressions for the critical volume, pressure, and temperature.

Based on investigation[30] of interactions of a rigid sphere with another rigid sphere and half-space using the Lennard–Jones potential, by their integrating over the surfaces and volumes, respectively, the analytical forms of surface tractions and total force between two rigid spheres were obtained. First of them can be used for the description of adhesive contact between rigid and elastic bodies. The FVT (Free Volume Theory) extended to explicitly include the hard-sphere character of colloidal depletants into the free volume fraction expression was used[31] as a basis for comprehensive calculations performed to predict the phase behavior of large spherical colloids mixed with small spherical ones acting as depletant.

The parameters of the Mie–Lennard–Jones pair potential for nearest bond-forming fullerenes or interfullerene interaction in fcc-fullerites were determined[32] from the data on correlation revealed between fullerene mass and corresponding fullerite properties. The experimentally observed fact that under the same conditions C_{70} fullerite is more stable than C_{60} was explained[33] by calculation equilibrium bond energy between C_{60}–C_{60} and C_{70}–C_{70} fullerene pairs using the potential energy curve for interaction between two identical hollow spherical molecules, which is given with formula including the Lennard–Jones potential parameters.

It has been emphasized[34] that pair-wise interatomic potentials presentable in analytical form serve for powerful theoretical tools to model various nanosystems: nanoparticles, nanotubes, fullerenes, AFM (Atomic Force Microscope) probes, etc. In particular, using so-called equilibrium MD simulations the effect of electrostatic interactions influence on heat transfer mechanism and interfacial properties was investigated[35] for the hexagonal boron nitride−water system Kapitza resistance in nanoscale planar (nanosheet) and cylindrical (nanotube) geometries. A water molecule was imaged by the simple point charge model due to its reliability, precision, and relatively low computational cost. An optimized Tersoff potential was used to model the h-BN sheet–tube interactions. And the pairwise interactions between atoms or ions were described by adding Coulomb and Lennard–Jones potentials. The optimum structure of some materials at the nanoscale, including boron-based clusters, was modeled[36] by employing standard and ab initio MD simulations. The used instantaneous forces on atoms were calculated from Lennard–Jones, van der Waals, Coulomb, etc. potentials.

2.2 Ab initio potentials

The ZRPM (Zero-Range Potential Model) treats[37,38] the atomic and molecular potentials as short-range potential-wells with a shallow energy level near the continuum spectrum boundary. It is a schematic description of these potentials for cases (e.g., negative atomic ion), in which the internal structure details are not too significant. The basic idea of the approach is to replace the wave equation solution inside the well by a boundary condition at its center. The single potential well model useful for atoms can be directly generalized for the case of molecules, when there are several potential wells.

Dolgonosov[39] has proposed an atomic electron gas model together with the generalized charges theory and the subsequent development of the interatomic interactions theory for the ab initio description of covalent bonding and van der

Waals forces, as well as complex molecules adsorption on homogeneous surfaces.

In the studies of Shukla and Eliasson[40–42], it was pointed out a short-range attractive force between two ions screened by degenerate electron gas in an unmagnetized plasma. At quantum scale, due to that force it can arise ordered ion structures such as ion clusters or Coulomb ion lattices, as well as the phase separations in dense quantum plasmas, e.g., from solid to liquid–vapor. Corresponding electric potential is attributed to the quantum statistical pressure and the quantum Bohm potential, as well as the electron exchange and electron correlations due to electron-1/2 spin.

Bonding in the excited alkali dimers involving resonant ionic, covalent and steric interactions was studied[43] by ab initio calculation for case of second, third, fourth and fifth $^1\Sigma_u^+$-states of lithium diatomic molecule Li_2. In particular, the corresponding potential energy curves were obtained and applied for high resolution laser spectroscopy.

Usually, conformational profiles are obtained with DFT methods, using of which is time-consuming when the molecules are relatively large or there are many molecules of interest. Wang *et al.*[44] compared several possible alternatives to this traditional approach, including a neural network potential. It was found that a sequential geometry optimization with the semiempirical method and single-point energy high-level DFT calculation can provide satisfactory conformational energy profiles hundreds of times faster.

The concept of electronegativity χ reformulated within DFT has acquired a central place in chemical reactivity due to its special relationship with the chemical potential μ:$\mu = -\chi$, and definition of so-called local electronegativity viewed as the functional variation of the system energy with respect to the electronic density in a given potential environment. On the one hand, the chemical hardness concept realization within the conceptual DFT is approached with perspective of electronegativity and hardness equalization of atoms in molecules. On the other hand, the maximum hardness principle presents a relation with the chemical stability of the hardness concept. In light of these concepts and inverse relation between hardness and polarizability, the minimum polarizability principle has been proposed by Kaya and Putz[45]. Additionally, this review includes applications of the chemical hardness concept. Elucidating the quantum nature of the chemical bond is fundamental to establishing the directed chemical synthesis of new compounds with predefined properties and reactivity aiming at specific interactions. The structures, intermolecular interactions, and energy of some energetic materials crystal models were comparatively predicted based on MD quantum chemical simulations[46]. Detecting the intermolecular interactions would provide fundamental insights for the energetic materials crystal engineering.

Electronic structure of charged defects in crystals often is calculated in the supercell models, which include the jellium counter charges to maintain system's overall neutrality. However, the correction related to these artificially charges becomes paramount for low-dimensional crystals, where they may induce the spurious vacuum states. A corresponding self-consistent potential correction scheme was presented in the study of Silva *et al.*[47]. A problem of identification of parameters of the Mie–Lennard–Jones- and Morse-type pairwise interatomic potentials from the interaction between metal atom and graphene layer was considered by Rekhviashvili *et al.*[48] using the continuum approximation. The potential parameters were calculated by the DFT method from the equilibrium adsorption energy and distances in the adatom–graphene system. The advantage of this method is that the empirical combining rules are not used. The Mie–Lennard–Jones potential was found to be the most suitable for describing such interaction. The problem with the Morse potential is that the exponential function cannot equally correctly describe the attractive and repulsive forces.

2.3 Machine learning potentials

In ML schemes, the potentials of interaction between constituent atoms i and j and crystal molar energy can be represented in forms of $U_{ij}(r_{ij}) = \sum_k A_k / r_{ij}^k$ and $u = \sum_l \sum_{ij} \sum_k A_k / r_{ij}^k$, respectively. Here A_k is the constant, summation

is done over unit cells number l = 0, 1, 2, … and index i is assumed to refer to the atom in the cell with l = 0. In these lattice sums, the terms with indices k = 0, 1, 2 describe so-called long-range interactions, because corresponding volume integrals over whole space diverge. One has to calculate them only inside a finite sphere. The well-known Ewald method developed for the Coulomb part, k = 1, can be generalized to terms with k = 0, 1, 2, 3 as well. Below, a few recent examples of ML potentials development are given.

A machine learning scheme[49] for an unbiased and accurate representation of interatomic potentials is a combination of an artificial neural network and a simple approach for reconstruction of pair interatomic (e.g., Al–Al, He–He and Xe–Xe) potentials in elementary crystals providing accuracy comparable with ab initio ones, but at a small computational cost. This method can be applied to structures of real systems of atoms by MD simulations. A highly automated approach to dataset construction and then building a potential for elementary aluminum, called as ANI-Al, was presented in the research of Smith *et al.*[50]. In this active scheme, the ML potential under development is used to drive non-equilibrium MD simulations with time-varying applied temperatures. Whenever a configuration is reached for which the ML uncertainty is large, new QC data is collected. The ML model is periodically retrained on all the available QC data. The final ANI-Al potential makes accurate predictions of radial distribution function in melt, liquid-solid coexistence curve, and crystal properties such as defect energies and barriers. It was performed a 1.3×10^6 atom shock simulation and shown that corresponding force predictions agree well with DFT calculations.

In the study of Mortazavi *et al.*[51], it was shown that ML interatomic potentials trained over short ab initio MD trajectories enable ab initio multiscale modeling, in which DFT is hierarchically bridged to efficiently simulate macroscopic structures. It was demonstrated that such approach can efficiently predict the lattice thermal conductivity of graphene and borophene pristine phases, as well as graphene–borophene interfaces. Thus, ML interatomic potentials enable ab initio multiscale modeling via hierarchical employment of DFT/MD/FE simulations for computational design of novel nanostructures. The structural properties of amorphous boron nitride a-BN doped with varying amount of carbon C were modeled[52] by generating versatile force fields using ab initio and designing realistic disordered BN:C ML simulations.

The recent review[53] highlights developments in the use of ML to evaluate chemical properties such as partial atomic charges, dipole moments, spin and electron densities, and chemical bonding, as well as to obtain a reduced QC description. There is overviewed several neural network architectures, their predictive capabilities, generality and transferability, and illustrated their applicability to various chemical properties. It is emphasized that ML molecular representations resemble QC analogues demonstrating the ability of the models to capture the underlying physics. It is also discussed how ML models can describe non-local quantum effects. The observed trends demonstrate that this field is evolving towards physics-based models augmented by ML.

3. Charge density and potential distributions in boron atom

Atom is a bounded system of electrically interacting electric charges—positive nucleus and negative electrons. So, to calculate potential energy of interaction between two atoms in fully theoretical manner, one needs their detailed electronic structure, including the explicit expressions for electric charge density and electric field potential distributions in interacting atoms.

Recently, it has been demonstrated[54,55] that electronic structure of any bounded system of atoms—molecules, clusters or even condensed matter—with a good accuracy can be calculated within the semiclassical approximation expressing electric SCF (Self Consistent Field) affecting atomic electrons by Coulomb-like (pseudo) potentials. Based on electric charge density and electric field potential radial distributions in constituent atoms obtained in this way, one can construct semiclassical interatomic pair potentials needed

for calculating the important physical characteristics of any bounded system of atoms.

In such type semiclassical approximation, for ground-state electronic configuration $1s^2 2s^2 2p^1$, the radial wave functions $R_k(q_k(r))$ of five electrons,

$$k = 1, 2, 3, 4, 5 \tag{1}$$

of an isolated electrically neutral boron B atom with nuclei centered at the origin, $\vec{r} = 0$, are

$$R_1(q_1(r)) = \sqrt{\left(\frac{Z_1}{r_B}\right)^3} 2\exp\left(-\frac{q_1(r)}{2}\right) \tag{2}$$

$$R_2(q_2(r)) = \sqrt{\left(\frac{Z_2}{r_B}\right)^3} 2\exp\left(-\frac{q_2(r)}{2}\right) \tag{3}$$

$$R_3(q_3(r)) = \sqrt{\left(\frac{Z_3}{r_B}\right)^3} \frac{1}{2\sqrt{2}}(2 - q_3(r))\exp\left(-\frac{q_3(r)}{2}\right) \tag{4}$$

$$R_4(q_4(r)) = \sqrt{\left(\frac{Z_4}{r_B}\right)^3} \frac{1}{2\sqrt{2}}(2 - q_4(r))\exp\left(-\frac{q_4(r)}{2}\right) \tag{5}$$

and

$$R_5(q_5(r)) = \sqrt{\left(\frac{Z_5}{r_B}\right)^3} \frac{1}{2\sqrt{6}} q_5(r)\exp\left(-\frac{q_5(r)}{2}\right) \tag{6}$$

Here the variables

$$q_k(r) = \frac{2Z_k}{n_k}\frac{r}{r_B} \tag{7}$$

stand for radial wave functions' arguments. The constant

$$r_B = \frac{\hbar^2}{e^2 m} \approx 0.53\ \text{Å} \tag{8}$$

is the Bohr radius,

$$n_1 = n_2 = 1 \tag{9}$$

$$n_3 = n_4 = 2 \tag{10}$$

and

$$n_5 = 2 \tag{11}$$

are the electron orbitals' principal quantum numbers, while the parameters Z_k equal to

$$Z_{12} \equiv Z_1 = Z_2 \approx 4.69 \tag{12}$$

$$Z_{34} \equiv Z_3 = Z_4 \approx 2.76 \tag{13}$$

and

$$Z_5 \approx 1.48 \tag{14}$$

respectively. These are the nucleus effective charge numbers, respectively, for $1s^2$, $2s^2$, and $2p^1$ electrons bounded in boron atom. They could be considered for known numerical quantities.

On the one hand, in the Coulomb-like intra-atomic field the classical orbit radii r_k of electrons or their characteristic displacements from the nucleus could be found from the relations:

$$\frac{r_k}{r_B} = \frac{n_k^2}{Z_k} \tag{15}$$

On the other hand, the nuclear charge radii of boron stable isotopes ^{10}B and ^{11}B with charge number of $Z = 5$ approximately equal to[56]

$$R_5 \approx 2.4 \times 10^{-5}\ \text{Å} \tag{16}$$

$$\frac{R_5}{r_B} \approx 2.2 \times 10^{-6} \tag{17}$$

and, consequently, in the boron atom the nucleus electric charge radius is negligible in comparison with electrons' characteristic displacements from it:

$$\frac{R_5}{r_k} \ll 1 \tag{18}$$

These relations meet a key assumption of the semiclassical method used that atomic nucleus could be considered as point electric charge.

The squared semiclassical radial wave functions,

$$R_{12}^2(r) \equiv R_1^2(r) = R_2^2(r) = \frac{4Z_{12}^3}{r_B^3}\exp\left(-\frac{2Z_{12}r}{r_B}\right)$$

(19)

$$R_{34}^2(r) \equiv R_3^2(r) = R_4^2(r) = \frac{Z_{34}^3}{8r_\mathrm{B}^3}\left(2-\frac{Z_{34}r}{r_\mathrm{B}}\right)^2 \exp\left(-\frac{Z_{34}r}{r_\mathrm{B}}\right) = \left(\frac{Z_{34}^3}{2r_\mathrm{B}^3}-\frac{Z_{34}^4 r}{2r_\mathrm{B}^4} + \frac{Z_{34}^5 r^2}{8r_\mathrm{B}^5}\right)\exp\left(-\frac{Z_{34}r}{r_\mathrm{B}}\right)$$

(20)

and

$$R_5^2(r) = \frac{Z_5^3}{24r_\mathrm{B}^3}\left(\frac{Z_5 r}{r_\mathrm{B}}\right)^2 \exp\left(-\frac{Z_5 r}{r_\mathrm{B}}\right) = \frac{Z_5^5 r^2}{24r_\mathrm{B}^5}\exp\left(-\frac{Z_5 r}{r_\mathrm{B}}\right)$$

(21)

determine the semiclassical electrical charge density distribution in the isolated boron atom:

$$\rho_\mathrm{B}(\vec{r}) = 5e\delta(\vec{r}) - \frac{e}{4\pi}\sum_{k=1}^{k=5} R_k^2(|\vec{r}|) = e\left(5\delta(\vec{r}) - \frac{2R_{12}^2(r) + 2R_{34}^2(r) + R_5^2(r)}{4\pi}\right)$$

(22)

Here, the first term containing Dirac delta-function $\delta(\vec{r})$ stands for positive charge density of point-like nucleus with charge number of $Z = 5$ and the second term is negative charge density of electron cloud.

From the corresponding semiclassical electrical charge density radial distribution.

$$\rho_\mathrm{B}(\vec{r}) = e\left(5\delta(\vec{r}) - \frac{2Z_{12}^3}{\pi r_\mathrm{B}^3}\exp\left(-\frac{2Z_1 r}{r_\mathrm{B}}\right) - \left(\frac{Z_{34}^3}{4\pi r_\mathrm{B}^3}-\frac{Z_{34}^4 r}{4\pi r_\mathrm{B}^4} + \frac{Z_{34}^5 r^2}{16\pi r_\mathrm{B}^5}\right)\exp\left(-\frac{Z_{34}r}{r_\mathrm{B}}\right) - \frac{Z_5^5 r^2}{96\pi r_\mathrm{B}^5}\exp\left(-\frac{Z_5 r}{r_\mathrm{B}}\right)\right)$$

(23)

the Poisson's equation determines that of the electrical field potential,

$$\varphi_\mathrm{B}(r) = e\left(\left(\frac{2}{r}+\frac{2Z_{12}}{r_\mathrm{B}}\right)\exp\left(-\frac{2Z_{12}r}{r_\mathrm{B}}\right) + \left(\frac{2}{r}+\frac{3Z_{34}}{2r_\mathrm{B}}+\frac{Z_{34}^2 r}{2r_\mathrm{B}^2} + \frac{Z_{34}^3 r^2}{4r_\mathrm{B}^3}\right)\exp\left(-\frac{Z_{34}r}{r_\mathrm{B}}\right) + \left(\frac{1}{r}+\frac{3Z_5}{4r_\mathrm{B}}+\frac{Z_5^2 r}{4r_\mathrm{B}^2} + \frac{Z_5^3 r^2}{24r_\mathrm{B}^3}\right)\exp\left(-\frac{Z_5 r}{r_\mathrm{B}}\right)\right)$$

(24)

in the boron atom centered at the origin: $\vec{r} = 0$.

4. Potential energy of B–B interaction

In general, an atom electrically interacting with another one affects its electric charge density and, consequently, electric field potential distributions. However, in the vicinity of interatomic chemical bond equilibrium length such redistributions are relatively small: both in finite and infinite bounded systems of atoms electric charge density and electric field potential distributions can be approximated by the simple superposition of corresponding distributions in constituent atoms in their isolated states, when they are localized in structure sites.

Assuming electric charge density and related electric field potential redistributions in electrically interacting pair of boron atoms displaced at vector $\vec{a}$ (**Figure 1**) to be negligible, the semiclassical potential energy of such interaction can be found as volume integral:

$$U_{\mathrm{B-B}}(a) = \iiint d^3\vec{r}\,\varphi_\mathrm{B}(r)\rho_\mathrm{B}(\vec{r}-\vec{a})$$

(25)

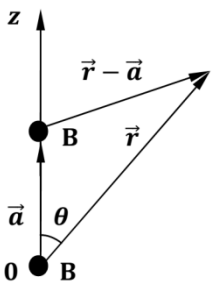

Figure 1. To calculation of B–B pair potential.

The trivial integration over the polar angle $0 \le \phi \le 2\pi$ yields the following result:

$$U_{\mathrm{B-B}}(a) = 5e^2\left(\left(\frac{2}{a}+\frac{2Z_{12}}{r_\mathrm{B}}\right)\exp\left(-\frac{2Z_{12}a}{r_\mathrm{B}}\right)+\left(\frac{2}{a}+\frac{3Z_{34}}{2r_\mathrm{B}}+\frac{Z_{34}^2a}{2r_\mathrm{B}^2}+\frac{Z_{34}^3a^2}{4r_\mathrm{B}^3}\right)\exp\left(-\frac{Z_{34}a}{r_\mathrm{B}}\right)\right.$$
$$\left.+\left(\frac{1}{a}+\frac{3Z_5}{4r_\mathrm{B}}+\frac{Z_5^2a}{4r_\mathrm{B}^2}+\frac{Z_5^3a^2}{24r_\mathrm{B}^3}\right)\exp\left(-\frac{Z_5a}{r_\mathrm{B}}\right)\right)$$
$$-e^2\int_0^\infty dr\,r^2\left(\left(\frac{2}{r}+\frac{2Z_{12}}{r_\mathrm{B}}\right)\exp\left(-\frac{2Z_{12}r}{r_\mathrm{B}}\right)+\left(\frac{2}{r}+\frac{3Z_{34}}{2r_\mathrm{B}}+\frac{Z_{34}^2r}{2r_\mathrm{B}^2}+\frac{Z_{34}^3r^2}{4r_\mathrm{B}^3}\right)\exp\left(-\frac{Z_{34}r}{r_\mathrm{B}}\right)\right.$$
$$\left.+\left(\frac{1}{r}+\frac{3Z_5}{4r_\mathrm{B}}+\frac{Z_5^2r}{4r_\mathrm{B}^2}+\frac{Z_5^3r^2}{24r_\mathrm{B}^3}\right)\exp\left(-\frac{Z_5r}{r_\mathrm{B}}\right)\right)$$
$$\times\int_0^\pi d\theta\sin\theta\left(\frac{4Z_{12}^3}{r_\mathrm{B}^3}\exp\left(-\frac{2Z_1\sqrt{r^2-2ar\cos\theta+a^2}}{r_\mathrm{B}}\right)\right.$$
$$+\left(\frac{Z_{34}^3}{2r_\mathrm{B}^3}-\frac{Z_{34}^4\sqrt{r^2-2ar\cos\theta+a^2}}{2r_\mathrm{B}^4}\right.$$
$$\left.+\frac{Z_{34}^5(r^2-2ar\cos\theta+a^2)}{8r_\mathrm{B}^5}\right)\exp\left(-\frac{Z_{34}\sqrt{r^2-2ar\cos\theta+a^2}}{r_\mathrm{B}}\right)$$
$$\left.+\frac{Z_5^5(r^2-2ar\cos\theta+a^2)}{48r_\mathrm{B}^5}\exp\left(-\frac{Z_5\sqrt{r^2-2ar\cos\theta+a^2}}{r_\mathrm{B}}\right)\right) \tag{26}$$

As for integration over the azimuthal angle $0 \le \theta \le \pi$, it can be conducted via two successive transformations into new integration variables x and t:

$$\cos\theta = x \tag{27}$$

and

$$r^2 - 2arx + a^2 = t^2 \tag{28}$$

finally leading to the form

$$U_{\mathrm{B-B}}(a) = 5e^2\left(\left(\frac{2}{a}+\frac{2Z_{12}}{r_\mathrm{B}}\right)\exp\left(-\frac{2Z_{12}a}{r_\mathrm{B}}\right)+\left(\frac{2}{a}+\frac{3Z_{34}}{2r_\mathrm{B}}+\frac{Z_{34}^2a}{2r_\mathrm{B}^2}+\frac{Z_{34}^3a^2}{4r_\mathrm{B}^3}\right)\exp\left(-\frac{Z_{34}a}{r_\mathrm{B}}\right)\right.$$
$$\left.+\left(\frac{1}{a}+\frac{3Z_5}{4r_\mathrm{B}}+\frac{Z_5^2a}{4r_\mathrm{B}^2}+\frac{Z_5^3a^2}{24r_\mathrm{B}^3}\right)\exp\left(-\frac{Z_5a}{r_\mathrm{B}}\right)\right)$$
$$-\frac{e^2}{r_\mathrm{B}a}\int_0^\infty dr\,r\left(\left(\frac{2}{r}+\frac{2Z_{12}}{r_\mathrm{B}}\right)\exp\left(-\frac{2Z_{12}r}{r_\mathrm{B}}\right)+\left(\frac{2}{r}+\frac{3Z_{34}}{2r_\mathrm{B}}+\frac{Z_{34}^2r}{2r_\mathrm{B}^2}+\frac{Z_{34}^3r^2}{4r_\mathrm{B}^3}\right)\exp\left(-\frac{Z_{34}r}{r_\mathrm{B}}\right)\right.$$
$$\left.+\left(\frac{1}{r}+\frac{3Z_5}{4r_\mathrm{B}}+\frac{Z_5^2r}{4r_\mathrm{B}^2}+\frac{Z_5^3r^2}{24r_\mathrm{B}^3}\right)\exp\left(-\frac{Z_5r}{r_\mathrm{B}}\right)\right)\times\left(J_{12}(r)+J_{34}(r)+J_5(r)\right) \tag{29}$$

where

$$J_{12}(r) = \frac{4Z_{12}^3}{r_\mathrm{B}^2}\int_{|r-a|}^{r+a}dt\,t\exp\left(-\frac{2Z_{12}t}{r_\mathrm{B}}\right)$$
$$= Z_{12}\left(\left(1+\frac{2Z_{12}|r-a|}{r_\mathrm{B}}\right)\exp\left(-\frac{2Z_{12}|r-a|}{r_\mathrm{B}}\right)-\left(1+\frac{2Z_{12}(r+a)}{r_\mathrm{B}}\right)\exp\left(-\frac{2Z_{12}(r+a)}{r_\mathrm{B}}\right)\right) \tag{30}$$

$$J_{34}(r) = \int_{|r-a|}^{r+a} dt\, t \left(\frac{Z_{34}^3}{2r_B^2} - \frac{Z_{34}^4 t}{2r_B^3} + \frac{Z_{34}^5 t^2}{8r_B^4}\right) \exp\left(-\frac{Z_{34} t}{r_B}\right) =$$
$$= \frac{Z_{34}}{4}\left(\left(1 + \frac{Z_{34}|r-a|}{r_B} - \frac{Z_{34}^2|r-a|^2}{2r_B^2} + \frac{Z_{34}^3|r-a|^3}{2r_B^3}\right) \exp\left(-\frac{Z_{34}|r-a|}{r_B}\right)\right.$$
$$\left. - \left(1 + \frac{Z_{34}(r+a)}{r_B} - \frac{Z_{34}^2(r+a)^2}{2r_B^2} + \frac{Z_{34}^3(r+a)^3}{2r_B^3}\right) \exp\left(-\frac{Z_{34}(r+a)}{r_B}\right)\right) \quad (31)$$

and

$$J_5(r) = \frac{Z_5^5 t^2}{48 r_B^4} \int_{|r-a|}^{r+a} dt\, t \exp\left(-\frac{Z_5 t}{r_B}\right)$$
$$= \frac{Z_5}{8}\left(\left(1 + \frac{Z_5|r-a|}{r_B} + \frac{Z_5^2|r-a|^2}{2r_B^2} + \frac{Z_5^3|r-a|^3}{6r_B^3}\right) \exp\left(-\frac{Z_5|r-a|}{r_B}\right)\right.$$
$$\left. - \left(1 + \frac{Z_5(r+a)}{r_B} + \frac{Z_5^2(r+a)^2}{2r_B^2} + \frac{Z_5^3(r+a)^3}{6r_B^3}\right) \exp\left(-\frac{Z_5(r+a)}{r_B}\right)\right) \quad (32)$$

are the definite radial, $0 \le r \le \infty$, integrals.

Thus, semiclassical approximation has allowed us to express the boron–boron pair potential

$$U_{B-B} = U_{B-B}(a) \quad (33)$$

in dependence on interatomic distance a by a radial integral.

Schematic view of an interatomic pair potential U as a function of the interatomic distance r is shown in **Figure 2**. Here r_0 is the equilibrium interatomic distance, i.e., bond length in corresponding diatomic molecule, and U_0 is its binding energy (not corrected for relative atomic vibrations zero-point energy).

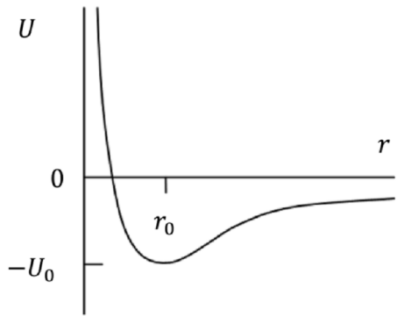

Figure 2. Schematic of interatomic pair potential.

The integration over the radius is possible to conduct in elementary functions, although it will give the result in a cumbersome analytical form. Therefore, it seems that for the practical applications of the constructed B–B potential often it will be necessary to convert it in a numerical form.

It is clear that the same goal can be achieved by the direct numerical integration.

5. Discussion and conclusion

Further work aims to convert the obtained in integral form semiclassical B–B potential function into analytical and/or numerical forms, which will allow to determine the B–B bond's parameters such as bond length, dissociation energy, frequency of relative atomic vibrations, etc. They should be compared with currently available data given below.

To the best our knowledge for the first time the fully theoretical pair potential energy curves for low-lying energy states of diboron molecule B_2 were constructed[57] by so-called complete-active-space SCF method at the multi-reference CI (Configuration Interaction) level of theory. The potential curves of ground and some of low-lying excited electronic states of B_2 neutral molecule and B_2^+ positive ion were also obtained[58] by using another CI approach. The B_2^+ cation ground state showed a rather shallow potential curve with a bond length of 2.13 Å and vibration quantum of 0.052 eV, when compared with B_2 neutral ground state with that of 1.59 Å and 0.131 eV, respectively. In result of bonding electron loss, the B_2^+ molecular ion ground-state dissociation energy of 1.94 eV was found to be significantly smaller than that of B_2: 3.06 eV. Later, same authors by extensive multi-reference CI calculations were constructed[59] B_2 and B_2^+ potential curves yielding

the following sets of parameters 1.59 Å, 2.75 eV, 0.131 eV and 2.12 Å, 1.90 eV, 0.052 eV, respectively. And according to the one more multi-reference CI study[60], the ground-state curve parameters of B_2 such as bond length, dissociation energy and two atoms relative vibration quantum are of 1.60–1.61 Å, 2.70–2.78 eV and 0.128–0.129 eV, respectively. First principles quadratic CI method was used[61] to calculate the equilibrium potential energy curves of ground and low-lying excited electronic states of B_2 and B_2^+. The corresponding analytical potentials were constructed by the fitting calculation results to the Murrell–Sorbie potential energy function. Curve parameters obtained for B_2 and B_2^+ were, respectively, 1.62 Å, 3.14 eV, 0.125 eV and 2.18 Å, 1.69 eV, 0.052 eV.

A non-SCF DFT based construction of non-orthogonal TB (Tight-Binding) matrix elements for B–B, N–N, B–N, B–H and N–H systems within the framework of the LCAO (Linear Combination of Atomic Orbitals) formalism was presented[62] using the LDA (Local Density Approximation). Despite the simplicity of the scheme considering only two-center Hamiltonian integrals and overlap matrix elements, the method has been proven to be sufficiently accurate and transferable to all scale B–B(N,H) structures from small clusters and molecules to crystalline solids and solid surfaces. The calculation of forces from these TB potentials is straightforward and allows an application of the method to MD simulations of structure formation in complex BNH systems.

For the B_2 molecule ground-state interatomic potential, the energy curve was also constructed[63,64] within a quasi-classical approach. The obtained in such way curve's parameters are as follows: equilibrium bond length of 1.78 Å, dissociation energy of 2.80 eV, and vibration quantum of 0.130 eV.

Most of NIST's IPR potentials are presented in efficient "universal" shifted Lennard–Jones model for all KIM API supported species developed by Elliott and Akerson in 2015[65]. Cohesive energy graphs generated for each elemental crystals supported by the model show the cohesive energy versus volume-per-atom for four mono-atomic cubic phases: sc (simple cubic), bcc, fcc, and diamond-like. The curve with the lowest minimum is the ground state of the crystal, if stable. Point is that the crystal structure is enforced in these calculations, so the phase may not be stable. In particular, cohesive energy graphs are available for elemental boron, i.e., B–B, and some boron-containing systems: B–N, B–Hf, B–Zr and B–C–N. The local nature of different types of boron–boron bonds—B·B, B–B, B=B and B≡B—from the topological analysis of ELF (Electron Localization Function) perspective was investigated[66] in number of boron-containing molecules.

As for the experimental parameters of B–B pair interatomic potential curve, they are available in the reference book[67]: 1.59 Å, 3.09 eV, 0.130 eV. Currently, for neutral diboron B_2 molecule in ground state configuration $(\sigma 1s)^2(\sigma^* 1s)^2(\sigma 2s)^2(\sigma^* 2s)^2(\pi 2p)^2$ bond length and bond energy are estimated[68] as 0.159 nm and 3.00 eV, respectively.

In similar way, one can construct different semiclassical interatomic pair potentials to characterize the nanomaterials containing not only boron, but some other chemical elements as well. For example, results obtained on the basis of semiclassical boron–nitrogen, i.e., B–N, potential for pristine and doped hexagonal boron nitride h-BN nanotubes prospective for toxic gas sensors can be compared with DFT ones on their electrical sensitivity toward ethyl benzene C_8H_{10} and phosphine PH_3 molecules[69,70].

In summary, introduced in this work semiclassical boron–boron potential integral function allowing presentation both analytically or numerically will serve as a useful tool to characterize all-boron and boron-rich nanomaterials atomic and electron structures fully theoretically and predict their main physical properties.

Conflict of interest

The author declared no conflict of interest.

References

1. Becker R, Chkhartishvili L, Martin P. Boron, the new graphene? Vacuum Technology & Coating 2015; 16(4): 38–44.

2. Chkhartishvili L. All-boron nanostructures. In: Kharisov BI, Kharissova OV, Ortiz–Mendez U (editors). CRC concise encyclopedia of nanotechnology. Boca Raton: CRC Press; 2016. p. 53–69.
3. Li D, Gao J, Cheng P, *et al*. 2D boron sheets: Structure, growth, and electronic and thermal transport properties. Advanced Functional Materials 2019; 1904349: 1–32. doi: 10.1002/adfm.201904349.
4. Tian Y, Guo Z, Zhang T, *et al*. Inorganic boron-based nanostructures: Synthesis, optoelectronic properties, and prospective applications. Nanomaterials 2019; 9(538): 1–22. doi: 10.3390/nano9040538.
5. Boustani I. Molecular modeling and synthesis of nanomaterials. Applications in carbon- and boron-based nanotechnology. Cham: Springer Nature; 2020.
6. Matsuda I, Wu K (editors). 2D boron: Boraphene, borophene, boronene. Cham: Springer Nature; 2021.
7. Alexandrova AN, Boldyrev AI, Zhai HJ, *et al*. All-boron aromatic clusters as potential new inorganic ligands and building blocks in chemistry. Coordination Chemistry Reviews 2006; 250(21–22): 2811–2866. doi: 10.1016/j.ccr.2006.03.032.
8. Chkhartishvili L. Quasi-planar elemental clusters in pair interactions approximation. Open Physics 2016; 14(1): 617–620. doi: 10.1515/phys-2016-0070.
9. Chkhartishvili L. Boron quasi-planar clusters. A mini-review on diatomic approach. In: 2017 IEEE 7th International Conference on Nanomaterials: Applications & Properties; 2017 Sep 10–15; Odessa. New York: IEEE; 2017. p. 1–5.
10. Chkhartishvili L. Relative stability of planar clusters B_{11}, B_{12}, and B_{13} in neutral- and charged-states. Characterization and Application of Nanomaterials 2020; 3(2): 73–80. doi: 10.24294/can.v3i2.761.
11. Chkhartishvili L. Relative stability of boron planar clusters in diatomic molecular model. Molecules 2022; 27(1469): 1–20. doi: 10.3390/molecules27051469.
12. Levitin V. Interatomic bonding in solids. Fundamentals, simulation, and applications. Weinheim: Wiley-VCH Verlag GmbH & Co. KGaA; 2014.
13. Gennes PG, Brochard–Wyart F, Quere D. Capillarity and wetting phenomena. Drops, bubbles, pearls, waves. New York: Springer; 2004.
14. Marques JMC, Prudente FV, Pirani F. Intermolecular forces: From atoms and molecules to nanostructures. Molecules 2022; 27(3072): 1–3. doi: 10.3390/molecules27103072.
15. Zhigilei LV. Course MSE 4270/6270: Introduction to atomistic simulations. Charlottesville: University Virginia; 2013.
16. Interatomic Potentials Repository. NIST; 2023.
17. Magomedov MN. Izucheniye mezhatomnogo vzaimodejstviya, obrazovaniya vakansij i samodiffuzii v kristallakh (Russian) [Study of interatomic interaction, formation of vacancies and self-diffusion in crystals]. Moscow: Physical-Mathematical Literature Press; 2010.
18. Muser MH, Sukhomlinov SV, Pastewka L. Interatomic potentials: Achievements and challenges. Advances in Physics X 2023; 8(1): 2093129. doi: 10.1080/23746149.2022.2093129.
19. Magomedov MN. The energy of interatomic interaction for crystals of elements of the carbon subgroup. High Temperature 2005; 43(2): 192–202. doi: 10.1007/s10740-005-0060-1.
20. Magomedov MN. On the brittleness of elementary semiconductors. Physics of the Solid State 2023; 65(2): 205–210. doi: 10.21883/PSS.2023.02.55401.521.
21. Magomedov MN. A method for the parameterization of the pairwise interatomic potential. Physics of the Solid State 2020; 62(7): 1126–1131. doi: 10.1134/S1063783420070136.
22. Magomedov MN. Study of the fcc–bcc phase transition in an Au–Fe alloy. Physics of the Solid State 2022; 64(13): 2093–2101. doi: 10.21883/PSS.2022.13.52307.145.
23. Magomedov MN. Changing the parameters of vacancy formation and self-diffusion in various polymorphic modifications of iron. Technical Physics 2023; 68(2): 209–217. doi: 10.21883/TP.2023.02.55474.190-22.
24. Bjorkas C, Henriksson KOE, Probst M, *et al*. A Be–W interatomic potential. Journal of Physics: Condensed Matter 2010; 22(35): 352206. doi: 10.1088/0953-8984/22/35/352206.
25. Erokhin KM, Kalashnikov NP. Relationships of macroscopic characteristics of a solid with the binding energy of an ion in a metal lattice. Physics of the Solid State 2021; 63(7): 973–977. doi: 10.1134/S1063783421070064.
26. Poluektov YM. Dvukhatomnaya model' kvantovogo kristalla (Russian) [The biatomic model of a quantum crystal]. Low Temperatures Physics 2008; 34(4–5): 459–469.
27. Sdobnyakov NY, Sokolov DN, Samsonov VM, *et al*. Gupta multiparticle potential study of the hysteresis of the melting and solidification of gold nanoclusters. Russian Metallurgy 2012; 2012(3): 209–214. doi: 10.1134/S0036029512030111.
28. Thomas SP, Dikundwar AG, Sarkar S, *et al*. The relevance of experimental charge density analysis in unraveling noncovalent interactions in molecular crystals. Molecules 2022; 27(12): 3690. doi: 10.3390/molecules27123690.
29. Rekhviashvili SSh, Bukhurova MM, Sokurov AA. Quantum crystal equation of state. Technical Physics Letters 2023; 49(2): 43–45. doi: 10.21883/TPL.2023.02.55369.19368.
30. Wu JJ. The interactions between spheres and between a sphere and a half-space, based on the Lennard–Jones potential. Journal of Adhesion Science and Technology 2012; 26(1–3): 251–269. doi: 10.1163/016942411X576130.
31. Opdam J, Schelling MPM, Tuinier R. Phase behavior of binary hard-sphere mixtures: Free volume theory including reservoir hard-core interac-

tions. The Journal of Chemical Physics 2021; 154(7): 074902. doi: 10.1063/5.0037963.
32. Magomedov MN. Interfullerene interaction and properties of fullerites. High Temperature 2005; 43(3): 379–390. doi: 10.1007/s10740-005-0076-6.
33. Nikonova RM, Lad'yanov VI, Rekhviashvili SSh, *et al*. Thermal stability of C_{60} and C_{70} fullerites. High Temperature 2021; 59(2–6): 179–183. doi: 10.1134/S0018151X21020103.
34. Bukhurova MM, Rekhviashvili SSh. Primenenie mezhatomnykh potentsialov vzaimodejstvia dlya modelirovaniya nanosistem (Russian) [Application of interatomic interaction potentials for the simulation of nanosystems]. Bulletin of the Kamchatka Regional Association Educational and Scientific Center (Physical and Mathematical Sciences) 2020; 33(4): 166–187. doi: 10.26117/2079-6641-2020-33-4-166-187.
35. Alosious S, Kannam SK, Sathian SP, *et al*. Effects of electrostatic interactions on Kapitza resistance in hexagonal boron nitride−water interfaces. Langmuir 2022; 38(29): 8783–8793. doi: 10.1021/acs.langmuir.2c00637.
36. Hassani N, Hassani MR, Neek-Amal M. Boron-based cluster modeling and simulations: Application point of view. In: Wongchoosuk C (editor). Characteristics and applications of boron. London: IntechOpen; 2022. p. 1–16.
37. Drukarev G. The zero-range potential model and its application in atomic and molecular physics. Advances Quantum Chemistry 1978; 11: 251–274. doi: 10.1016/S0065-3276(08)60239-7.
38. Demkov YN, Ostrovskii VN. Zero-range potentials and their applications in atomic physics. New York, London: Plenum Press; 1988.
39. Dolgonosov AM. Model' elektronnogo gaza i teorya obobshchennykh zaryadov dlya opisaniya adsorbtsii (Russian) [Electron gas model and generalized charges theory for describing interatomic forces and adsorption]. Moscow: Librokom Book House; 2009.
40. Shukla PK, Eliasson B. Novel attractive force between ions in quantum plasmas. Physical Review Letters 2012; 108: 165007. doi: 10.1103/PhysRevLett.108.165007.
41. Shukla PK, Eliasson B. Erratum: Novel attractive force between ions in quantum plasmas. Physical Review Letters 2012; 108: 219902. doi: 10.1103/PhysRevLett.108.219902.
42. Shukla PK, Eliasson B. Erratum: Novel attractive force between ions in quantum plasmas. Physical Review Letters 2012; 109: 019901. doi: 10.1103/PhysRevLett.109.019901.
43. Furudate MA, Hagebaum–Reignier D, Kim JT, *et al*. Resonant ionic, covalent bond, and steric characteristics present in $^1\Sigma_u^+$ states of Li_2. Molecules 2022; 27(11): 3514. doi: 10.3390/molecules27113514.
44. Wang Y, Walker BD, Liu C, *et al*. An efficient approach to large-scale ab initio conformational energy profiles of small molecules. Molecules 2022; 27(23): 8567. doi: 10.3390/molecules27238567.
45. Kaya S, Putz MV. Atoms-in-molecules' faces of chemical hardness by conceptual density functional theory. Molecules 2022; 27(24): 8825. doi: 10.3390/molecules27248825.
46. Liu Y, An C, Liu N, *et al*. Noncovalent interactions and crystal structure prediction of energetic materials. Molecules 2022; 27(12): 3755. doi: 10.3390/molecules27123755.
47. Silva MC, Lorke M, Aradi B, *et al*. Self-consistent potential correction for charged periodic systems. Physical Review Letters 2021; 126: 076401. doi: 10.1103/PhysRevLett.126.076401.
48. Rekhviashvili SSh, Bukhurova MM, Sokurov AA. Determination of pairwise interaction of atoms from the interaction of an adatom with graphene. Russian Journal of Inorganic Chemistry 2020; 65(9): 1373–1377. doi: 10.1134/S0036023620090132.
49. Dolgirev PE, Kruglov IA, Oganov AR. Machine learning scheme for fast extraction of chemically interpretable interatomic potentials. AIP Advances 2016; 6(8): 085318. doi: 10.1063/1.4961886.
50. Smith JS, Nebgen B, Mathew N, *et al*. Automated discovery of a robust interatomic potential for aluminum. Nature Communications 2021; 12: 1257. doi: 10.1038/s41467-021-21376-0.
51. Mortazavi B, Podryabinkinc EV, Roched S, *et al*. Machine-learning interatomic potentials enable first-principles multiscale modeling of lattice thermal conductivity in graphene/borophene heterostructures. Materials Horizons 2020; 9: 1–25. doi: 10.1039/D0MH00787K.
52. Kaya O, Colombo L, Antidormi A, *et al*. Revealing improved stability of amorphous boron-nitride upon carbon doping. Nanoscale Horizons 2023; 8(3): 1–7. doi: 10.1039/d2nh00520d.
53. Fedik N, Zubatyuk R, Kulichenko M, *et al*. Extending machine learning beyond interatomic potentials for predicting molecular properties. Nature Reviews Chemistry 2022; 6: 653–657. doi: 10.1038/s41570-022-00416-3.
54. Chkhartishvili L. On semi-classical approach to materials electronic structure. Journal of Material Science and Technology Research 2021; 8: 41–49. doi: 10.31875/2410-4701.2021.08.6.
55. Chkhartishvili L. How to calculate condensed matter electronic structure based on multi-electron atom semi-classical model. Condensed Matter 2021; 6(4): 46. doi: 10.3390/condmat6040046.
56. Maass B, Huther T, Konig K, *et al*. Nuclear charge radii of ^{10,11}B. Physical Review Letters 2019; 122: 182501. doi: 10.1103/PhysRevLett.122.182501.
57. Dupuis M, Liu B. The ground electronic state of B_2. The Journal of Chemical Physics 1978; 68(2): 2902–2910. doi: 10.1063/1.436088.
58. Bruna PJ, Wright JS. Strongly bound multiply excited states of B_2^+ and B_2. The Journal of Chemical Physics 1989; 91(2): 1126–1136. doi: 10.1063/1.457185.

59. Bruna PJ, Wright JS. Theoretical study of the ionization potentials of boron dimer. The Journal of Physical Chemistry 1990; 94(5): 1774–1781. doi: 10.1021/j100368a014.
60. Langhoff SR, Bauschlicher CW. Theoretical study of the spectroscopy of B_2. The Journal of Chemical Physics 1991; 95(8): 5882–5888. doi: 10.1063/1.461609.
61. Yang CL, Zhu ZH, Wang R, *et al*. Analytical potential energy functions of the neutral and cationic B_2. Journal of Molecular Structure 2001; 548(1–3): 47–52. doi: 10.1016/S0166-1280(01)00372-4.
62. Widany J, Frauenheim T, Kohler T, *et al*. Density-functional-based construction of transferable nonorthogonal tight-binding potentials for B, N, BN, BH, and NH. Physical Review B 1996; 53(8): 4443–4452. doi: 10.1103/PhysRevB.53.4443.
63. Chkhartishvili L, Lezhava D, Tsagareishvili O, *et al*. Parametry osnovnogo sostoyanya diatomicheskikh molekul B_2, BC, BN i BO (Russian) [Ground-state parameters of diatomic molecules B_2, BC, BN and BO]. Proceedings of the Georgian Police Academy 1999; 1: 195–300.
64. Chkhartishvili L, Lezhava D, Tsagareishvili O. Quasi-classical determination of electronic energies and vibration frequencies in boron compounds. Journal of Solid State Chemistry 2000; 154(1): 148–152. doi: 10.1006/jssc.2000.8826.
65. Elliott RS. Efficient 'universal' shifted Lennard-Jones model for all KIM API supported species developed by Elliott and Akerson (2015) v003. OpenKIM; 2018. doi: 10.25950/962b4967.
66. Mierzwa G, Gordon AJ, Berski S. The nature of the triple B≡B, double B=B, single B–B, and one-electron B·B boron-boron bonds from the topological analysis of Electron Localization Function (ELF) perspective. Journal of Molecular Structure 2020; 1221: 128530. doi: 10.1016/j.molstruc.2020.128530.
67. Huber KP, Herzberg H. Molecular spectra and molecular structure. IV. Constants of diatomic molecules. New York: Van Nostrand Reinhold Compay; 1979.
68. Tilley RJD. Understanding solids. The science of materials. New York: John Wiley & Sons; 2021.
69. Noei M, Ahmadaghaei N, Salari AA. Ethyl benzene detection by BN nanotube: DFT studies. Journal of Saudi Chemical Society 2017; 21(1): S12–S16. doi: 10.1016/j.jscs.2013.09.008.
70. Mohajeri S, Noei M, Salari AA, *et al*. Adsorption of phosphine on a BN nanosurface. Iranian Journal of Chemistry and Chemical Engineering 2018; 37(1): 39–45. doi: 10.30492/IJCCE.2018.26372.